DOI:
10.1039/D0BM00314J

Document Version
Peer reviewed version

Biomaterials Science

Accepted Manuscript

This article can be cited before page numbers have been issued, to do this please use: J. T. Wang, U. Martino, R. Khan, P. Southern, D. Tuncel and K. T. Al-Jamal, *Biomater. Sci.*, 2020, DOI: 10.1039/D0BM00314J.

ROYAL SOCIETY OF CHEMISTRY

rsc.li/biomaterials-science

View Article Online
DOI: 10.1039/D0BM00314J

ARTICLE

Engineering red-emitting multi-functional nanocapsules for magnetic tumour targeting and imaging

Received 00th January 20xx,
Accepted 00th January 20xx

DOI: 10.1039/x0xx00000x

Julie Tzu-Wen Wang,*[a] Umberto Martino, [a] Rehan Khan, [b] Paul Southern, [c] Dönüş Tuncel, *[b] and Khuloud T. Al-Jamal *[a]

In this work we describe the formulation and characterisation of red-emitting polymeric nanocapsules (NCs) incorporating superparamagnetic iron oxide nanoparticles (SPIONs) for magnetic tumour targeting. The self-fluorescent oligomers were synthesised and chemically conjugated to PLGA which was confirmed by NMR, FT-IR spectroscopy and mass spectrometry. Hydrophobic SPIONs were synthesised through thermal decomposition and their magnetic and heating properties were assessed by SQUID magnetometry and calorimetric measurements, respectively. Magnetic nanocapsules (*m*-NC) were prepared by single emulsification/solvent evaporation method. The in vitro cytotoxicity was examined in CT26 colon cancer cells. The formulated fluorescent *m*-NCs showed good stability and biocompatibility both in vitro and in vivo in CT 26 colon cancer models. Following intravenous injection, accumulation of *m*-NCs in tumour was observed by optical imaging. Higher iron content in the tumours exposed to magnetic field, compared to the contralateral tumours without the magnetic exposure in the same animal, further confirmed the magnetic tumour targeting *in vivo*. The overall results show that the engineered red-emitting *m*-NCs have a great potential as multifunctional nanocarriers for multi-model bioimaging and magnetic-targeted drug delivery.

Introduction

Magnetic nanoparticles have been widely explored for their potential application for cancer diagnosis or therapy. [1, 2] For example, they can be used as contrast agents for magnetic resonance (MR) imaging to distinguish neoplastic lesions from normal tissues, taking advantage of their intrinsic magnetic properties. They can also be utilised for magnetic drug delivery such as tumour-targeting. Superparamagnetic iron oxide nanoparticles (SPIONs) are particularly ideal with this regard since they can be highly magnetised to the specific site of action upon exposure to external magnetic field and no magnetisation is retained once the magnetic field is removed, avoiding agglomeration. [3] SPIONs are usually produced as hydrophobic ferrofluid solution and need to be coated or encapsulated to be water-dispersible for intravenous injection. We have previously developed polymeric magnetic nanocapsules (*m*-NCs) capable of triple-modal imaging (i.e. MR, optical and nuclear imaging)
. [4] NCs are nanoparticulate carriers composed of an oil core surrounded by a PEGylated-PLGA polymeric shell with lipophilic and/or hydrophilic surfactants present at the interface. These polymeric NCs served as a versatile platform with the capacity to load high amounts of water insoluble drug molecules/SPIONs/fluorescent probes into the oil core. [4-6] The polymeric formulation provided the protection against enzymatic degradation and conferred a greater physicochemical stability as a whole. Based on the enhanced permeability and retention (EPR) effect, the m-NCs were able to passively accumulate in solid tumours with leaky vasculature. [7, 8] The presence of SPION further facilitated magnetic targeting in tumours in mice when an external magnetic field was applied. [4, 7-9] As a result, with encapsulating an anticancer drug docetaxel, the *m*-NCs indeed significantly delayed tumour growth and reduced systemic side effects compared to the free drug. [9]

In previous studies, we were able to dynamically visualise magnetic targeting of m-NCs with tumour and its vasculature by optical imaging with the aid of infra-red fluorescent probes indocyanine green (ICG) [4] or 1,1-dioctadecyltetramethyl indotricarbocyanine Iodide (DiR) [7] incorporated into the oil phase of *m*-NC. Small organic fluorescent molecules can be used as imaging probes; however, they suffer from photo-bleaching and are therefore not suitable for long time imaging, especially *in vivo*. Recently, intrinsically fluorescent polymers, capable of forming nanoparticulate systems, have been proposed as a new type of fluorophores which can be used for *in vitro* cell labelling, *in vivo* live imaging and in image-guided drug delivery. [10-14] It was also shown that drug molecules can

[a] School of Cancer and Pharmaceutical Sciences, Faculty of Life Science & Medicine, King's College London, UK. E-mail: tzu-wen.wang@kcl.ac.uk, khuloud.al-jamal@kcl.ac.uk
[b] Department of Chemistry and UNAM–National Nanotechnology Research Centre, Bilkent University, Turkey. E-mail: dtuncel@fen.bilkent.edu.tr
[c] UCL Healthcare and Biomagnetics Laboratories, Royal Institution of Great Britain, London, UK.
Electronic Supplementary Information (ESI) available:

be loaded with high loading capacity due to hydrophobic effect and favourable π-π interaction between the drug molecules and the conjugated oligomer or polymer chains. [15, 16]

primary amine groups using PPh3 to provide Oligomer 2. Finally, PLGA was conjugated to Oligomer 2 through amide bond formation using DCC coupling reaction.

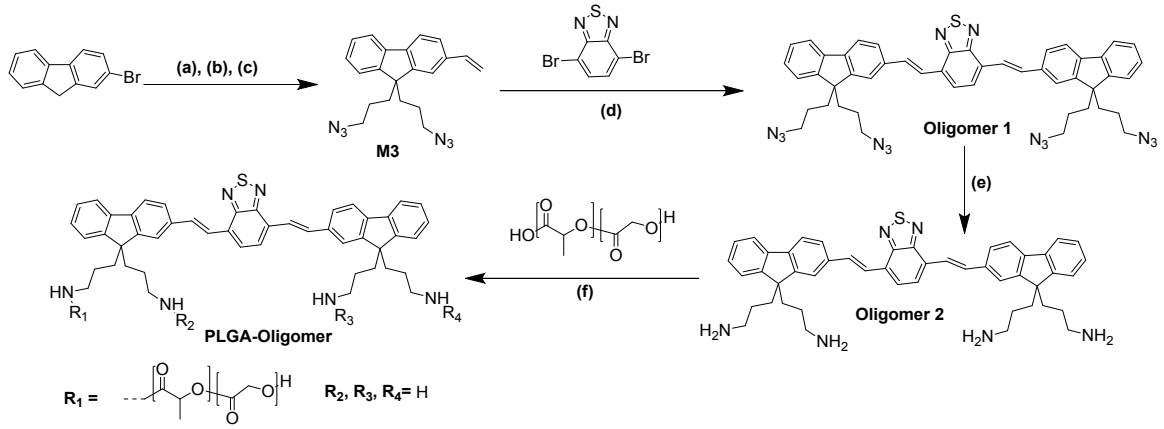

Scheme 1: Synthesis scheme for PLGA-Oligomer. (a) **M1:** 1,3-Dibromopropane, aq. NaOH (50%, w/w), tetra-butyl ammonium bromide (TBAB), 80 °C, 64%, (b) **M2:** tributyl vinyltin, $Pd(Cl_2)(PPh_3)_2$, 2,6-di-tert-butyl phenol, toluene, 100 °C, 24 h, 90%, (c) **M3:** NaN_3, 60 °C, DMF, 24 h, 93%, (d) aq. K_2CO_3, $Pd(OAc)_2$, $Pd(PPh_3)_4$, DMF, 70 °C, 24 h, 45%, (e) PPh_3, THF, 25 °C, 24 h, 80%, (f) 1-Ethyl-3-(3-dimethylaminopropyl)carbodiimide (EDC), 4-dimethylaminopyridine (DMAP), 60 °C, DMF, 48 h, 78%.

Although conjugated polymer nanoparticles can provide high drug loading capacity, biodegradation of the large polymeric residues after the delivery can present some problems. To this end, conjugated oligomers are attractive because they have short chain and well-defined molecular weight. Moreover, they exhibit higher fluorescent quantum yield than their polymeric counterparts. [17, 18] However, one drawback is their lower drug loading capacity compared to polymer nanoparticles. Thus, in this work, we took a different approach and conjugated directly the carboxyl terminated PLGA to amine functionalised red-emitting fluorescent oligomer through amide bond formation. The formulation of m-NC with the encapsulation of SPIONs was optimised and characterised. The organ biodistribution profiles and ability for magnetic tumour targeting following intravenous injection were assessed *in vivo* in CT 26 colon cancer models by optical imaging and iron content quantification. The engineered self-fluorescent *m*-NCs were capable of *in vivo* optical imaging and magnetic tumour targeting.

Results and discussion

Synthesis and characterisation of Oligomer 1, Oligomer 2 and PLGA-Oligomer

The main text of the article should appear here with headings as appropriate. In order to synthesise PLGA-conjugated oligomer, firstly Oligomer 1 and Oligomer 2 were synthesised as shown in the reaction Scheme 1. Monomer 1 (M1) and monomer 2 (M2) were prepared as reported previously [18] and subsequently bromide groups of M2 were substituted by azides to obtain M3. Thereafter, Pd-catalyzed Heck coupling reaction between M3 and 4,7-dibromobenzo[c]-1,2,5-thiadiazole afforded Oligomer 1. In order to have suitable functional groups to link covalently with the carboxyl terminated PLGA, azide groups of Oligomer 1 were reduced to

Due to the high molecular weight of PLGA (Av. MW, 18 kDa) compared to Oligomer 2 (MW, 745 Da), only one arm of the Oligomer 2 was functionalised. Unreacted Oligomer 2 and PLGA were removed by precipitating PLGA-Oligomer solution in THF into large excess of water-methanol mixture.

Monomers and oligomers were characterised fully, and their characterization data are provided in the supporting information (Figure 1 and S1-S3). Formation of Oligomer 1 and 2 were confirmed by NMR (Figure 1 and S2A), FT-IR spectroscopy (Figure S2C and S3A) and mass spectrometry (Figure S2B and S3A). In the IR-spectrum of Oligomer 1 (Figure S2C), the peak due to azide stretching at 2100 cm-1 disappears upon reduction of azide groups into amines to form Oligomer 2 (Figure S3A). Figure 1 compares the ^{1}H-NMR spectra of Oligomer 1, Oligomer 2 and PLGA-Oligomer. ^{1}H-NMR spectrum of PLGA-Oligomer shows the peaks of PLGA protons and some peaks from the aliphatic protons of Oligomer 2. The peaks belong to aromatic protons of Oligomer 2 are not clearly seen because of the dominance of PLGA peaks. Another reason for this

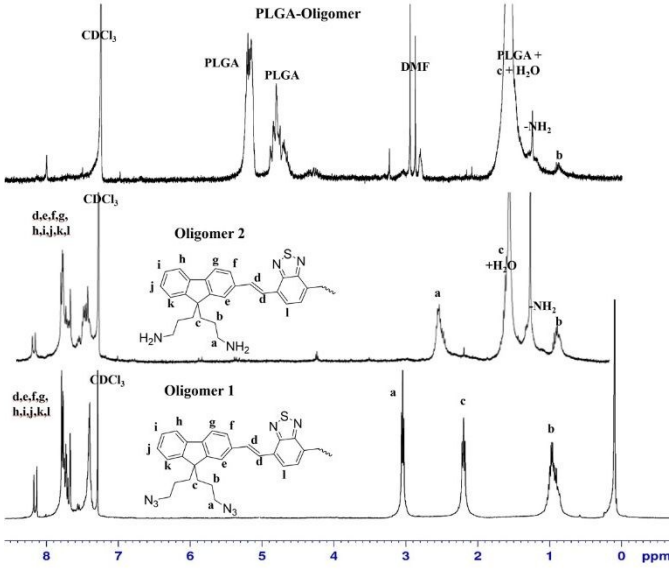

Figure 1: ^{1}H-NMR (400 MHz, $CDCl_3$, 25°C) spectra of Oligomer 1, 2 and PLGA-Oligomer.

could be due to a decrease in the mobility of aromatic backbone of the Oligomer 2 caused by the attachment of a bulky PLGA arm.

SPION synthesis and characterisation

SPIONs were synthesised through a high-temperature organic phase decomposition of an iron precursor. [19, 20] In contrast to the widely used co-precipitation method pioneered by Massart *et al*. with reactions taken place at room temperature, [21] the high-temperature decomposition method was reported to be able to provide a greater control on the final size of nanoparticles with a narrower size distribution. [22] Carrying out nucleation at 200 °C and grown reaction under reflux at ~300°C separately is the key to yield monodisperse and highly crystalline magnetic nanoparticles. In the present study, different durations for nucleation and growth (30 min to 2 h) were applied to optimise the synthesis of Fe_3O_4 magnetic nanoparticles (NP1 – NP5, Table S1). By SQUID (superconducting quantum interference device) magnetometry, the obtained hysteresis loops normalised by saturation magnetisation were identical among all NPs, indicating that varying the time of nucleation and growth did not significantly affect the magnetic properties of the synthesised Fe_3O_4 NPs significantly (Figure S4A). The heating capability of the magnetic nanoparticles can be assessed by quantification of the intrinsic loss power (ILP) values, the normalised energy dissipation rates, facilitating direct comparison when measurements were performed under different conditions. [23] Typical ILP values for iron oxide nanoparticles were reported in the range from 0.17 to 3.12 nHm^2/kg [24] or below 5 nHm^2/kg. [25] The obtained ILP values (Figure S4B, and Table S1) were relatively low (0.02-0.04 nHm^2/kg) as expected due to small particle size, estimated smaller than 10 nm. [26] Thermogravimetric analysis (TGA) was carried out to measure the oleic acid coating on NP1-NP5 which is indicated as weight loss % shown in Table S1. It has been reported that the amount of surfactant adsorption on the Fe_3O_4 nanoparticles decreased when the size of nanoparticles increased. [20] Since NP1 exhibited the lowest weight loss and the highest ILP value among all, further seed mediated growth (SMG) reaction (see Methods), known to increase the diameter of nanoparticles by ~2 nm per cycle, [19] was performed on NP 1 to increase SPIONs size and presumably their heating ability. The same synthesis condition (i.e. nucleation for 1 h and growth for 30 min) was followed for SMG reaction. For comparison, a parallel approach was carried out to produce Fe/Co hybrid nanoparticles in a single step method which is expected to have enhanced heating property due to increased magnetic anisotropy. [27]

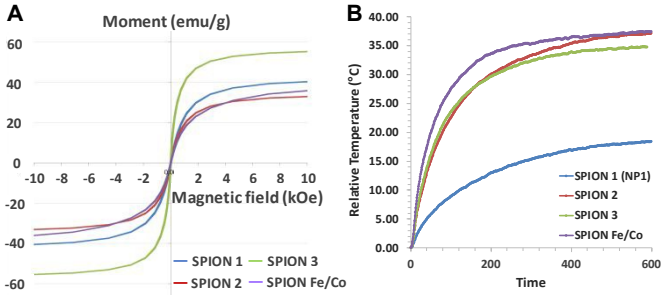

Figure 2: Characterisation of the SPIONs synthesised by seed mediated growth reaction (SMG) and SPION hybrid Fe/Co. (A) Magnetic property and **(B)** heating capacity assessments. Magnetization hysteresis curves were measured by SQUID magnetometry and normalised by the weight of the magnetic material. Calorimetric measurements were performed using a radio frequency amplifier.

Table 1: Heating properties of SPIONs

SPIONs	Intrinsic loss power (ILP, nHm^2/kg) [a]
SPION 1 (NP1)	0.04
SPION 2	0.27
SPION 3	0.53
SPION Fe/Co	0.18

[a] The calculation of ILP values were based on the iron content measured by ICP-MS and did not account for the oleic acid coating. The values were therefore lower than the actual values.

NP 1 is named SPION 1 hereafter and SPION 2-3 were prepared by subjecting NP 1 to further 1-2 cycles of SMG respectively. The magnetic and heating properties of SPION 1-3 and the hybrid SPION Fe/Co were assessed (Figure 2). No shift in hysteresis was present, indicating that their superparamagnetic behaviours were maintained, and their sizes are under the superparamagnetic/ferromagnetic threshold (Figure 2A). SPIONs produced by SMG exhibited significantly higher ILP values (0.271 and 0.533 nHm^2/kg for SPION 2 and SPION 3, respectively) than SPION 1 (0.043 nHm^2/kg) and the hybrid SPION Fe/Co (0.178 nHm^2/kg) (Table 1). Since its ILP value fell into the range reported in the literature, SPION 3 was chosen to formulate the magnetic polymeric nanocapsules in the subsequent studies.

PLGA nanocapsules formulation and characterisation

Nanocapsules were formulated by the emulsification/solvent evaporation method. Initial formulation was optimised using PLGA mixing with increasing amount of PLGA-Oligomer (10, 20 and 50 % of total polymer). The results of the size and zeta potential measurements of formulated nanocapsules are shown in Table S2. It was found that increasing the percentage of PLGA-Oligomer led to increased particle size and surface charge (less negative) and the nanocapsules made of 50 % PLGA-Oligomer was the largest in size (>300 nm) among the three nanocapsules. Nevertheless, all formulations showed good stability in which no significant changes in size and zeta potential were observed after storage at 4 °C for 1 week (data not shown). After purification by using PD-10 columns, tetrahydrofuran was added to the collected nanocapsules to break down the particles and dissolve the polymers. The optical properties of NC, Oligomer 2 and PLGA-Oligomer were assessed by UV-Vis spectroscopy and fluorimetry (Figure S5). It should be noted that NC were dispersed in PBS, while Oligomer 2 and PLGA-Oligomer were dissolved in THF. From the fluorescence spectra (Figure 5SB), Oligomer 2 and PLGA-Oligomer displayed the same emission maximum at 580 nm and there was a red shit for NC with the emission maximum at 590 nm. By measuring the fluorescence intensity of the PLGA-Oligomer extracted from nanocapsules (calibration curves shown in Figure S5C), nearly 100 % recovery was obtained in the polymer solutions, indicating that entire amount of

View Article Online
DOI: 10.1039/D0BM00314J

Table 2: Physicochemical characterisation of different formulations of fluorescent NC and *m*-NCs prepared by the emulsification/solvent evaporation method.

Name	PLGA-PEG	PLGA-Oligomer	SPION 3	Diameter (nm)*	PDI*	Zeta potential (mV)*	EE %†
NC	80%	20%		236.3 ± 4.8	0.208	-13.9 ± 1.2	-
***m*-NC**	80%	20%	2.5 mg	251.1 ± 3.8	0.221	-13.2 ± 0.2	89.3

* Measurements were performed by dynamic light scattering in 10 mM NaCl (n=3).

† **Iron content was determined by ICP-MS (n=3)**

PLGA-Oligomer was incorporated into the nanocapsule formulations (data not shown). Nanocapsules composed of 20 % PLGA-Oligomer
of total polymers, with compromised properties in terms of size, stability and fluorescence intensity, were chosen for further PLGA-PEG magnetic nanocapsule formulation.

Magnetic PLGA-PEG nanocapsules formulation and characterisation

Magnetic polymeric nanocapsules consisted of PLGA-PEG (80 %), PLGA-Oligomer (20%) and SPION 3 were formulated using the emulsification/solvent evaporation method. The formulated nanocapsules are named *m*-NC hereafter. The counterpart formulation without SPIONs was also formulated, named NC hereafter. The composition, size and zeta potential measurements of NC and *m*-NC are shown in Table 2. Inclusion of SPIONs slightly increased the size but does not affect the zeta potential of the nanocapsules. The size of NC and *m*-NC was in the range of 230-250 nm, larger than the *m*-NC reported in our previous study (~200 nm) . [4] High encapsulation efficiency (EE %) of SPIONs was determined by ICP-MS in which nearly ~90 % SPION EE% was achieved.

***In vitro* cytotoxicity studies**

The cytotoxic effect of NC and m-NC was assessed in CT26 cells using MTT assay prior to *in vivo* studies. As expected from our previous study, [9] no significant toxicity was observed in cells treated with either NC or *m*-NC up to the polymer concentration of 100 µg/ml for 72 h.

***In vivo* optical imaging with magnetic targeting**

For *in vivo* studies, NC and *m*-NC solutions were concentrated to 10 x and buffered with 10X PBS for injection. Physicochemical characterisation showed the size of NC or *m*-NC was within the range of 210-240 nm (Table S3). Prior to *in vivo* imaging, the optical properties of NC and *m*-NC solutions were tested on a well plate at different concentrations up to 500 µg/ml using IVIS Lumina III optical imaging system. This was performed considering that the previously reported oligomer has never been used for *in vivo* imaging. [18] A linear regression was measured for both NC and *m*-NC solutions at 500 nm/620 nm as excitation/ emission wavelength. Expectedly, due to the presence of SPIONs, quenching of fluorescence was observed in *m*-NC as signals were lower compared to NC at the same polymer concentration which was more obvious at the higher concentrations (Figure S6).

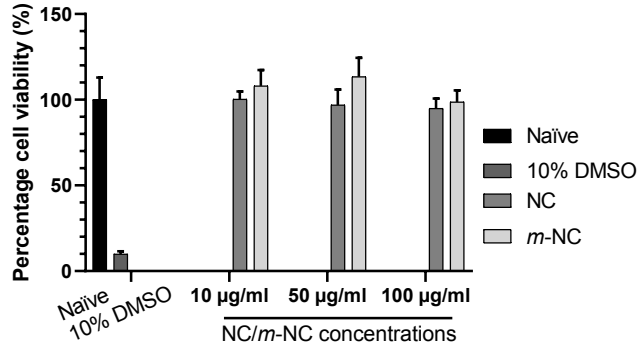

Figure 3: *In vitro* cytotoxicity assessments. CT26 cells were incubated with NC, and *m*-NC at the polymer concentration of 10, 50 and 100 µg/ml. Cell viability was assessed by MTT assay after 72 h incubation.

CT26 tumour-bearing balb/c mice were intravenously injected with NC or *m*-NC. A permanent magnet (0.515 T) was placed at one side of the tumours (TU$^+$) for 1 h. The contra-lateral tumour (TU$^-$) was

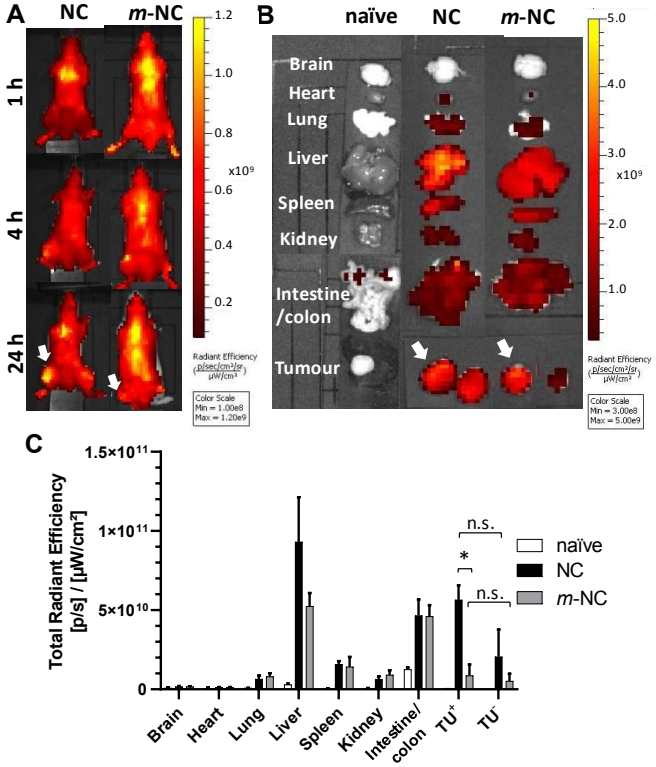

Figure 4: *In vivo* whole-body optical imaging and *ex vivo* biodistribution of NC and *m*-NC in CT26 tumour-bearing Balb/c mice after intravenous administration. (A) Representative whole-body images from dorsal views of mice at 1, 4 and 24 h post injection. **(B)** Representative *ex vivo* images of tissues excised at 24 h post injection. **(C)** Semi-quantitative analysis of uptake of NC and *m*-NCs in major tissues at 24 h post injection. Balb/c mice were transplanted subcutaneously with CT26 tumours at the lower flanks. When tumours reached ~7-8 mm in diameter, mice were *i.v.* injected with NC or *m*-NC (250 mg polymer/kg and 50 mg SPION/kg). Magnetic field was applied by placing a permanent magnet (0.515 T) at the tumour on the left side (TU$^+$) for 1 h (pointed by arrows). All images were obtained by IVIS Lumina III optical imaging system (λ_{ex}: 500; λ_{em}: 620 nm). Data were analyzed by Living Image® 4.3.1 Service Pack 2 software. Data present as mean ± S.D. (n=3). * p =0.01. (one-way ANOVA)

View Article Online
DOI: 10.1039/D0BM00344J

used as an internal control where no magnet was applied. Animals behaved normally without weight changes up to 24 h after receiving single intravenous injection of NC or m-NC. Increasing signals in tumours were observed over time up to 24 h although differences between TU^+ and TU^- were not obvious through whole-body imaging (Figure 4A). *Ex vivo* images of tissues excised at 24 h post injection confirmed the uptake of NC and *m*-NC in tumours (Figure 4B and S7). NC and *m*-NC had similar biodistribution patterns in general in which the particles accumulate in liver as well as other organs such as spleen, lung, kidney and intestine/colon. Quantitative analysis showed higher but insignificant signals detected in the tumours that had received 1 h magnet exposure (TU^+) compared to non-treated tumours (TU^-) in both cases of mice injected with NC or *m*-NC (Figure 4C). Decreased fluorescence for m-NC compared to NC group was observed, more significantly for TU+ treatment (p =0.01). This suggested the possibility of false negative results due to fluorescence quenching of the oligomer by SPION. It was deemed necessary to verify magnetic targeting by another method based on quantification of SPION by ICP-MS.

Quantification of the iron content in tissues by ICP-MS

ICP-MS analysis of iron content in tissues was further performed to assess the magnetic targeting in tumours considering that fluorescence of the oligomer was significantly quenched by SPION. Samples from naïve mice was also processed to obtain the intrinsic iron levels in these tissues. Figure 5 presents the iron content per g of tissues. In the mice injected with *m*-NC, the highest amount of iron was detected in spleen and liver which already contains the highest intrinsic iron (black bars). The intrinsic amount of iron in CT26 tumours were low (32.8 µg Fe/g of tumour) whilst a significant increase was observed in the tumours from mice injected with *m*-NC (zoom-in graph, Figure 5). Moreover, the tumours exposed to magnet for 1 h (TU^+) showed a significantly higher iron content than

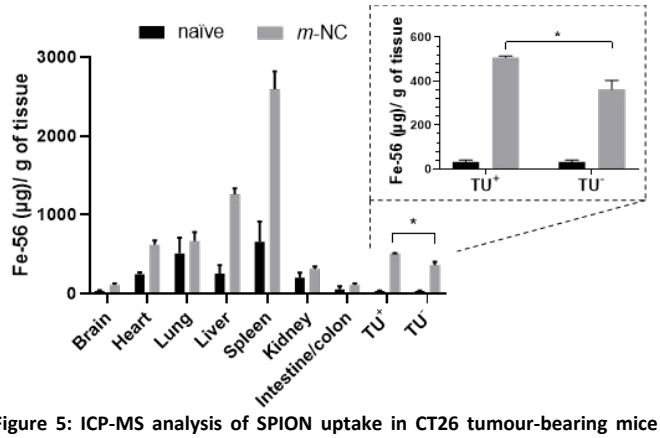

Figure 5: ICP-MS analysis of SPION uptake in CT26 tumour-bearing mice treated with *m*-NC. CT26-bearing Balb/c mice were i.v. injected m-NC (250 mg polymer/kg and 50 mg SPION/kg) and a permanent magnet (0.515 T) was applied to the tumour on one side (TU+) but not the other (TU-) for 1 h. At 24 h post injection, major organs and tumours were excised and proceeded with ICP-MS analysis as described in Methods. The data are expressed as iron content per g of tissues (dried weight) as mean±S.D. (n=3). *p = 0.04 (one-way ANOVA).

the tumours without magnet (TU^-) (507.6 ± 6.7 vs 362.0 ± 41.9 µg Fe/g, p=0.04). The results indicate the magnetic targeting effects on increasing the tumour uptake of *m*-NC. The fact *m*-NC reached tumour and achieved magnetic targeting with increased tumour uptake also suggest *m*-NC was stable enough *in vivo* after intravenous injection.

The multifunctional features of SPIONs have shown great promise in a wide range of biomedical applications. Moreover, many SPION-based nanoconstructs have been developed in which SPIONs were encapsulated or integrated with other materials to improve their hydrophilicity and biocompatibility. [28, 29] The present study demonstrated an effective and robust approach to encapsulate high amount of hydrophobic SPIONs in the hydrophobic compartment of the polymeric emulsion. The NC and m-NC developed in this study share many common features with the NC formulations published in our previous studies. [4, 7, 9] Apart from the inclusion of fluorescent PLGA-Oligomer and the replacement of SPIONs with the heating property, the choice of other excipients (e.g. PLGA-PEG, oil, surfactant), the quantities, and the formulation method and parameters were intended to remain unchanged to inherit the excellent fundamental physiochemical properties and the favourable *in vivo* behaviours. Indeed, the resulting NC/m-NC exhibit typical characteristics for coil-cored PEGylated NC including good colloidal stability, high SPION loading, and prolonged blood circulation thus passively enhanced tumour uptake. The resulting stable magnetic nanocapsules indeed exhibited improved water dispersity, prolonged blood circulation, and little or no toxicity *in vitro* and *in vivo* which are inherited from the characteristics of the PLGA-PEG polymers. By substitution of 20 % PLGA-PEG polymers with the red-emitting macromolecule conjugate consisting of an oligomer backbone with PLGA polymer chains, the engineered self-luminescent NCs and *m*-NCs enabled direct visualisation of their kinetic tumour accumulation over time after administration by *in vivo* optical imaging. This is different from our previous studies using conventional approaches either encapsulating or labelling with fluorescent probes for NC/m-NC in which the labelling stability and dissociation of the dye from the nanocarriers should be taken into account while assessing biodistribution profiles by imaging. [4, 7] Autofluorescence from tissues are expected which is mainly in green and red regions if excited by blue light. Considering the excitation for the fluorescent NC and *m*-NC at 500 nm (blue light), the obtained emission signals at 620 nm were rather satisfactory. In fact, the pilot in silico imaging in a well-plate has indirectly predicted the capability of the formulated *m*-NC for *in vivo* detection. The highest dose tested in the well-plate (500 µg/ml) was equivalent to 1 % injection dose (ID) for the *in vivo* studies (i.e. 1 % ID contains 50 µg of polymer) whose signals of $1x10^{10}$ photos/sec were distinct from background fluorescence and the likelihood of tissue autofluorescence signals usually below 10^9 photos/sec (Figure S6). The fluorescent PLGA-Oligomer and its nanocapsule formulation seemed to exhibit relatively high signal-to-noise ratio, indicating the capability for optical imaging *in vivo* or in clinic.

Hyperthermia is a promising tumour treatment and studies have developed magnetic nanoparticles for hyperthermia by means of photothermal ablation agent when irradiated with a NIR laser [30] or induce magnetic hyperthermia in the presence of an alternating magnetic field. [31] The SPIONs synthesised in

the present study displayed desirable heating properties, the evident magnetic tumour targeting has opened up a feasible future application of the developed *m*-NCs as a hyperthermia agent.

Conclusions

In conclusion, the resultant fluorescent m-NCs showed desirable magnetic and heating properties and exhibited good stability and biocompatibility both *in vitro* and *in vivo*. Following intravenous injection, accumulation of m-NCs in tumour was observed by optical imaging. Higher iron content in the tumours exposed to magnetic field, compared to the contralateral tumours without the magnetic exposure in the same animal, further confirmed the magnetic tumour targeting *in vivo*. The developed red-emitting functionalised m-NCs have a great potential as image-guided delivery system capable of magnetic-induced heating. Evaluation on the ability of the developed *m*-NC for hyperthermia and encapsulation chemotherapeutic drug will be the next stage studies.

Experimental

Materials

All the chemicals used were analytical grade, obtained from commercial suppliers and used as received without further purification. D/L-lactide/glycolide copolymer 75/25 ($PLGA_{18KDa}$-COOH) was purchased from Purac Biomaterials (Netherlands). Soybean lecithin (Epikuron 140 V) was a kind gift from Cargill Pharmaceuticals (USA). D/L-lactide/glycolide copolymer 75/25 ($PLGA_{18KDa}$-COOH) was purchased from Corbion Biomaterials (PURASORB® products, the Netherlands). PLGA-NH-PEG was synthesised as previously described [5]. Tween® 80 was obtained from Fisher Scientific Ltd (UK). Iron(III) acetylacetonate, Cobalt(II) avetylacetonate, 1,2 tetradecanediole, oleylammine, oleic acid, sodium chloride, castor oil, toluene, and benzyl ether were purchased from Sigma-Aldrich (UK). Black 96 well-plates were purchased from Fisher Scientific Ltd (UK). Disposable polystyrene cuvettes (for size and PDI) or capillary cells (for zeta potential) (Malvern Instrument, UK). PD-10 desalting column was obtained from GE Healthcare Life Sciences (UK). Gibco cell culture reagents including RPMI-1640 medium, fetal bovine serum (FBS), Glutamax™, non-essential amino acids, penicillin/streptomycin, Trypsin/EDTA, phosphate buffered saline (PBS) were purchased from Thermo Fisher Scientific Inc. 3-(4, 5-dimethylthiazol-2-yl)-2, 5-diphenyltetrazolium bromide (MTT) was purchased from Sigma-Aldrich (UK).

Synthesis of 9,9-bis(3-azidopropyl)-2-vinyl-9*H*-fluorene (M3)

2-bromo-9,9-bis(3-bromopropyl)-9*H*-fluorene and (M1) 9,9-bis(3-bromopropyl)-2-vinyl-9*H*-fluorene (M2) were synthesized as reported previously. [18] NaN_3 (400 mg, 6.15 mmol) was suspended in 10 mL of DMSO in round bottom flask and 9,9-bis(3-bromopropyl)-2-vinyl-9H-fluorene (M2) (600 mg, 1.38 mmol) was added into the flask. The reaction mixture was stirred at 60 °C for 24 h. After completion of the reaction, the solvent was removed under reduced pressure. The residue was washed with water several times and the collected solid was dried under reduced pressure. Yield: 460 mg, 93%. ^{1}H NMR (400 MHz, $CDCl_3$, 25 °C) δ ppm: 0.88-0.96 (m, 4H), 2.11-2.15 (t, 4H), 2.98-3.02 (t, 4H), 5.30-5.32 (d, 1H), 5.81-5.86 (d, 1H), 6.79-6.86 (m, 1H), 7.35-7.73 (m, 7H).

Synthesis of Oligomer 1

9,9-bis(3-azidopropyl)-2-vinyl-9H-fluorene (516 mg, 1.44 mmol) and 4,7-dibromobenzo[c][1,2,5]thiadiazole (207 mg, 0.72 mmol) were placed in a two-neck round bottom flask and dried under vacuum for 30 min. 10 mL dry and degassed dimethylformamide (DMF) was added and stirred to complete dissolution. Aqueous solution of K_2CO_3 (486 mg, 3.51 mmol) was added into the flask. The mixture was subjected to freeze-thaw-pump cycle for 3 times to remove oxygen. Catalytic amount of $Pd(OAc)_2$ (25.3 mg, 0.11 mmol) and $Pd(PPh_3)_4$ (26 mg, 0.02 mmol) were added under N_2 flow and the reaction mixture was heated to 70 °C for 24 h while constant stirring and under N_2 flow. After completion of the reaction, the solvent was removed under reduced pressure. The crude product was dissolved in dichloromethane (DCM) and extracted with water for several times. The organic phase was dried and further purified by column chromatography using diethyl ether as an eluent. Yield: 423 mg, 45 %. ^{1}H NMR (400 MHz, $CDCl_3$, 25 °C) δ ppm: 0.87-1.00 (m, 8H), 2.08-2.13 (m, 8H), 2.97-3.05 (d, 8H), 7.00-7.87 (m, 20H). ^{13}C NMR (400 MHz, $CDCl_3$, 25 °C) δ ppm: 23, 30, 38, 52, 54, 119, 120, 120.53, 121, 122, 123, 124, 126, 127, 128, 129.12, 134.1, 138, 141, 142, 149, 160. ESI-MS (m/z): Calcd. for C48H44N14S [M+H]+ :849.36, found: 849.36.

Synthesis of Oligomer 2

Oligomer 1 (200 mg, 0.236 mmol) was dissolved in tetrahydrofuran (THF) (10 mL) and then the solution of PPh_3 (370 mg, 1.48 mmol) in THF (5 mL) was added. The resulting mixture was stirred for 24 h at room temperature. Water (10 mL) was then added and stirred for 24 h. THF was removed under reduced pressure and the precipitates were collected by filtration. The solid was washed with diethyl ether several times and then dried under reduced pressure. Yield: 140 mg, 80%. ^{1}H NMR (400 MHz, $CDCl_3$, 25 °C) δ ppm: 0.87-1.00 (m, 8H), 1.5-1.8 (m, 8H), 2.5 (m, 8H), 7.00-7.87 (m, 20H). ESI-MS (m/z): Calcd. for C48H52N6S [M+H]+ :745.40, found: 745.40

Synthesis of PLGA-Oligomer

Oligomer 2 (70 mg, 0.094 mmol) was dissolved in dry DMF (6 mL) and 1-ethyl-3-(3-dimethylaminopropyl)carbodiimide (EDC) (73 mg, 0.47 mmol) and 4-dimethylaminopyridine (DMAP) (29 mg, 0.24 mmol) were added. The mixture was stirred for 5 min before adding PLGA (300 mg). The resulting mixture was further stirred at 60 °C under N_2 (g) for 48 h. After the reaction was over, the solvent was removed under reduced pressure and the residue was washed with water several times and then dried in the *vacuo*. Yield: 290 mg, 78%.

NMR, LC-MS and UV-Vis characterisations and instrumentation

All ^{1}H and ^{13}C NMR spectra were recorded at room temperature using a Bruker Avance III 400 MHz NMR spectrometer. $CDCl_3$ purchased from Merck was used as NMR solvent. Chemical shifts

are reported in ppm. Mass analyses were done with Agilent 6210 LC/MS TOF mass spectrometer. Optical characterizations were performed by Cary 300 UV-Vis spectrophotometer and Cary Eclipse fluorescence spectrophotometer.

SPIONs synthesis

The synthesis of SPIONs was performed by an high-temperature degradation of Iron(III) acetylacetonate as reported in literature. [19, 20] $Fe(acac)_3$ (2 mmol), 1,2-tetradecanediol (10 mmol), oleic acid (6 mmol), oleylamine (6 mmol), and benzyl ether (20 mL) were mixed and magnetically stirred under N_2 flow. For the synthesis of NP1, the mixture was heated to 200 °C for 1 h (nucleation reaction) and then, under a blanket of nitrogen, heated to reflux (298 °C, grown reaction) for another 30 min. The black-brown mixture was cooled to room temperature by removing the heat source. After the thermo-degradation reaction under ambient conditions, ethanol (40 mL) was added to the mixture and monodisperse Fe_3O_4 nanoparticles were obtained after centrifugation. The retrieved Fe_3O_4 nanoparticles were dissolved in hexane in the presence of oleic acid (~0.05 mL) and oleylamine (~0.05 mL). Centrifugation (6000 rpm, 10 min) was applied to remove any undispersed residue. The product, oleic acid-capped Fe_3O_4 nanoparticles, was then precipitated with ethanol, centrifuged (6000 rpm, 10 min) to remove the solvent, and re-dispersed into hexane, yielding NP1 (SPION 1). Different nucleation and grown time were used to synthesise NP2-NP5 in which the details are described in Table S1. SPION 1 dispersed in hexane was used as the seed to grow larger SPIONs in the $Fe(acac)_3$ precursors solution. Following the same workup procedures (e.g. nucleation/growth reaction and purification) described above, bigger oleic acid-capped Fe_3O_4 nanoparticles, i.e. SPION 2 (2 SMG steps) and SPION 3 (3 SMG steps), were produced.

As a control, reaction of $Co(acac)_2$ and $Fe(acac)_3$ (molar ratio $Co(acac)_2$: $Fe(acac)_3$ was 1 : 4; 2 mM total metal salts) underwent 2 h nucleation and 1 h growth reaction, leading to hybrid $CoFe_2O_4$ nanoparticles which was also dispersed in hexane.

Superconducting quantum interference device (SQUID) magnetometry

The magnetic properties of the SPIONs were assessed by SQUID magnetometry. SPION samples (approx. 10 mg) were mounted using soft gelatin capsules and the magnetization curves were recorded at room temperature (300K) using a Quantum Design (San Diego, USA) MPMS-VSM between ± 7 Tesla.

Thermogravimetric Analysis (TGA)

The amount of oleic acid coating on the SPION was characterised by the thermogravimetric analysis (TGA) using TGA Q500 (TA instrument). About 10 mg of SPIONs was loaded into platinum pan and the measurement was pre-equilibrated at 80 °C and then heated from 100 °C to 800°C with a temperature ramp of 10 °C/min under compressed air atmosphere with balance and sample purge flow at 10 and 90 ml/min, respectively.

Heating capability measurement

Calorimetric measurements were made using a radio frequency amplifier (Thamway T162-5723B) with a frequency range of 500–1000 kHz. The resonant circuit further consisted of a 20-turn water-cooled solenoid with 8cm diameter. The maximum AC magnetic field amplitude that could be generated was 13 kA/m at 930 KHz. A round-bottom-shaped plastic sample holder was used and surrounded by layers of insulation to protect the sample against ambient heating from the coil. Temperature measurements were conducted with fibre-optic temperature probes.[23]

NC and *m*-NC formulation

NCs and *m*-NCs were synthesised by the single emulsification/solvent evaporation method. Briefly, PLGA-PEG and PLGA-Oligomer mixture (12.5 mg), castor oil (75 mg), soybean lecithin (25 mg) and SPIONs (2.5 mg) were dissolved in 2.5 ml dichloromethane. Different ratios of PLGA-PEG and PLGA-Oligomer (weight percentage 90 %:10 %, 80 %:20 % and 50 %:50 %, Table S2) were used to formulate *m*-NC. The organic phase was poured into an aqueous phase (5 ml, water) containing Tween® 80 (20 mg). The resultant dispersion was emulsified by ultra-sonication using a probe sonicator (Soniprep 150, UK) at 15 micro amplitude for 180 s in an ice bath, followed by organic phase evaporation in a chemical fume hood under stirring for 20 min. The formulated NCs and m-NC were purified by size-exclusion chromatography (PD-10 column) using deionised water as the eluent to remove any un-encapsulated SPION or materials that are lacking water solubility. The final volume of the NC and *m*-NC solutions was adjusted to 5 ml using a rotary evaporator at 40 °C.

Size and zeta measurements

The hydrodynamic size (Z-Average), polydispersity index (PDI) and Zeta potential of the formulated NCs and *m*-NCs were determined by NanoZS (Malvern Instrument, UK) using disposable square polystyrene cuvettes (Malvern Instrument, UK) for size and PDI, and disposable capillary cells (Malvern Instrument, UK) for Zeta potential at 25 °C. For size measurement, NC and m-NC solutions were diluted with deionised water or 10 mM NaCl. The Z-Average diameter and polydispersity index were presented as the average value of three measurements, with 15 runs within each measurement. Electrophoretic mobility was used to calculate the Zeta potential measurement. Three measurements were performed with 10-20 runs within each measurement.

SPION encapsulation efficiency measurements

The iron content in the hydrophobic SPIONs stock solutions and the SPION encapsulated in *m*-NCs were determined by inductively couple plasma mass spectrometry (ICP-MS) (Perkin Elmer SCIEX ICP mass spectrometer, ELAN DRC 6100, USA). Fe standards (Leeman Labs Inc., MA) were prepared in 20 % nitric acid to obtain a standard curve in the range of 10-10000 parts

View Article Online DOI: 10.1039/D0BM00344J

per billion with respect to Fe. Different concentrations of SPION and m-NC solutions were digested in 67% nitric acid and incubated overnight at 50 °C. The resulting solution was diluted with deionised water before measurement. Iron content in non-purified NC solutions and purified NC solutions was measured to calculate the SPION encapsulation efficiency (EE%) in *m*-NCs.

***In vitro* cytotoxicity**

CT26 murine colon carcinoma (CT26, ATCC®, CRL-2638TM) cells were cultured in RPMI-1640 medium supplemented with 10% FBS, 50 U/mL penicillin, 50 µg/mL streptomycin, 1 % GlutamaxTM and 1 % non-essential amino acids. Cells were routinely grown in 75 cm2 canted-neck tissue culture flasks and passaged twice a week using Trypsin/EDTA at 80 % confluency.

CT26 cells were seeded in 96-well plates and incubated with NC or m-NC in complete media in the concentration of polymer at 10, 50 and 100 µg/mL for 72 h. Cell viability was examined by MTT assay. Briefly, the culture medium was removed and replaced with 120 µL of MTT solution (at a concentration of 5 mg/mL in PBS with a further 1: 6 dilution in media prior to use). Cells were incubated further for 3 h. Medium was removed, and the formed formazan was solubilised in 200 µL of DMSO. The absorbance was read at 570 nm using a FLUO star OPTIMA plate reader (BMG Labtech). cell viability was calculated as a percentage of untreated control cells and expressed as mean ± S.D. (n=6).

Animals and the tumour model

All animal experiments were performed in compliance with the UK Animals (Scientific Procedures) Act 1986 and UK Home Office Code of Practice for the Housing and Care of Animals Used in Scientific Procedures (Home Office 1989). *In vivo* experimentation was adhered to the project licence approved by the King's College London animal welfare and ethical review body (AWERB) and UK Home Office. Female Balb/c mice aged 4-6 weeks were purchased from Envigo (UK) and used for all the *in vivo* experiments. CT26 cells were cultured as described above. Cells were harvested, resuspended in PBS and injected subcutaneously at the lower flanks of both sides of the mice.

Purified NC and *m*-NC solutions were further concentrated by 10 times using a rotary evaporator and were adjusted to become isotonic by adding 10x PBS buffer solution. Disk neodymium magnets (8 mm in diameter, first4magnet, UK) with surface magnetic field flux densities at 0.515 Tesla (0.5 T) were used for *in vivo* magnetic targeting studies.

***In vivo* optical imaging and organ biodistribution studies**

Biodistribution studies were carried out when the tumours reached an appropriate size (~7-8 mm in diameter). CT26-bearing mice were subcutaneously injected with NC or *m*-NC solutions (250 mg polymer/kg and 50 mg SPION/kg). Immediately after injection, one magnet was placed non-invasively over the surface of the tumour implanted on the left flank and retained using surgical tapes. The contralateral tumour on the right side was used as an internal negative control where no magnet was applied. The magnet was removed at 1 h post-injection of the NC or *m*-NCs. Optical imaging was performed using an IVIS® Lumina series III *In Vivo* Imaging Device (Caliper Life Sciences, Perkin Elmer, USA). Images of mice were captured at 1, 4 and 24 h post-injection. At 24 h post-injection, major organs (brain, heart, lung, liver, spleen, kidney, intestine/colon) and tumours were excised, weighed and imaged by IVIS Lumina III optical imaging system (500/620 nm excitation/emission wavelengths) to assess the accumulation in tissues semi-quantitatively.

The iron accumulation in tissues were assessed quantitatively using ICP-MS. Tissues were dried, weighed and digested in 67 % nitric acid and incubated overnight at 50 °C. The digested tissue solutions were diluted with deionised water and centrifuged at 4,000 × g for 30 min. The supernatants were transferred into new tubes for ICP-MS analysis described previously.

Statistics analysis

Statistical significance between groups was determined using one-way ANOVA. Differences were considered statistically significant when *p*-values were less than 0.05.

Conflicts of interest

The authors declare no competing financial interest.

Acknowledgements

The authors would like to thank the funding from British Council Newton Fund Institutional Links (337313). DT would like to thank TÜBİTAK (Grant No: 216Z123) for financial support.

References

1. Arruebo, M.; Fernández-Pacheco, R.; Ibarra, M. R.; Santamaría, J., Magnetic nanoparticles for drug delivery. *Nano Today* 2007, **2** (3), 22-32.
2. Wu, M.; Huang, S., Magnetic nanoparticles in cancer diagnosis, drug delivery and treatment. *Molecular and Clinical Oncology* 2017, **7** (5), 738-746.
3. Bakhtiary, Z.; Saei, A. A.; Hajipour, M. J.; Raoufi, M.; Vermesh, O.; Mahmoudi, M., Targeted superparamagnetic iron oxide nanoparticles for early detection of cancer: Possibilities and challenges. *Nanomedicine: Nanotechnology, Biology and Medicine* 2016, **12** (2), 287-307.
4. Bai, J.; Wang, J. T.-W.; Rubio, N.; Protti, A.; Heidari, H.; Elgogary, R.; Southern, P.; Al-Jamal, W. T.; Sosabowski, J.; Shah, A. M., Triple-modal imaging of magnetically-targeted nanocapsules in solid tumours in vivo. *Theranostics* 2016, **6** (3), 15.
5. El-Gogary, R. I.; Rubio Carrero, N.; Wang, J. T.-W.; Al-Jamal, W. T.; Bourgognon, M.; Kafa, H.; Naeem, M.; Klippstein, R.; Abbate, V.; Leroux, F., Polyethylene glycol conjugated polymeric

nanocapsules for targeted delivery of quercetin to folate-expressing cancer cells in vitro and in vivo. *ACS Nano* 2014.

6. Klippstein, R.; Wang, J. T.-W.; El-Gogary, R. I.; Bai, J.; Mustafa, F.; Rubio, N.; Bansal, S.; Al-Jamal, W. T.; Al-Jamal, K. T., Passively Targeted Curcumin-Loaded PEGylated PLGA Nanocapsules for Colon Cancer Therapy In Vivo. *Small* 2015, **11** (36), 4704-4722.

7. Bai, J.; Wang, J. T.-W.; Mei, K.-C.; Al-Jamal, W. T.; Al-Jamal, K. T., Real-time monitoring of magnetic drug targeting using fibered confocal fluorescence microscopy. *Journal of Controlled Release* 2016, **244**, 240-246.

8. Mei, K.-C.; Bai, J.; Lorrio, S.; Wang, J. T.-W.; Al-Jamal, K. T., Investigating the effect of tumor vascularization on magnetic targeting in vivo using retrospective design of experiment. *Biomaterials* 2016, **106**, 276-285.

9. Al-Jamal, K. T.; Bai, J.; Wang, J. T.; Protti, A.; Southern, P.; Bogart, L.; Heidari, H.; Li, X.; Cakebread, A.; Asker, D.; Al-Jamal, W. T.; Shah, A.; Bals, S.; Sosabowski, J.; Pankhurst, Q. A., Magnetic drug targeting: Preclinical in vivo studies, mathematical modeling, and extrapolation to humans. *Nano letters* 2016, **16** (9), 5652-60.

10. Feng, G.; Fang, Y.; Liu, J.; Geng, J.; Ding, D.; Liu, B., Multifunctional Conjugated Polymer Nanoparticles for Image-Guided Photodynamic and Photothermal Therapy. *Small* 2017, **13** (3), 1602807.

11. Li, D.-D.; Wang, J.-X.; Ma, Y.; Qian, H.-S.; Wang, D.; Wang, L.; Zhang, G.; Qiu, L.; Wang, Y.-C.; Yang, X.-Z., A Donor–Acceptor Conjugated Polymer with Alternating Isoindigo Derivative and Bithiophene Units for Near-Infrared Modulated Cancer Thermo-Chemotherapy. *ACS Applied Materials & Interfaces* 2016, **8** (30), 19312-19320.

12. Tuncel, D., π-Conjugated nanostructured materials: preparation, properties and photonic applications. *Nanoscale Advances* 2019, **1** (1), 19-33.

13. Xu, X.; Liu, R.; Li, L., Nanoparticles made of π-conjugated compounds targeted for chemical and biological applications. *Chemical Communications* 2015, **51** (94), 16733-16749.

14. Yu, J.; Rong, Y.; Kuo, C.-T.; Zhou, X.-H.; Chiu, D. T., Recent Advances in the Development of Highly Luminescent Semiconducting Polymer Dots and Nanoparticles for Biological Imaging and Medicine. *Analytical Chemistry* 2017, **89** (1), 42-56.

15. Gezici, Ö.; Durmaz, İ.; Bilget Güven, E.; Ünal, Ö.; Özgün, A.; Cetin-Atalay, R.; Tuncel, D., Dual functionality of conjugated polymer nanoparticles as an anticancer drug carrier and a fluorescent probe for cell imaging. *RSC Advances* 2014, **4** (3), 1302-1309.

16. Pennakalathil, J.; Özgün, A.; Durmaz, I.; Cetin-Atalay, R.; Tuncel, D., pH-responsive near-infrared emitting conjugated polymer nanoparticles for cellular imaging and controlled-drug delivery. *Polymer Chemistry* 2015, **53** (1), 114-122.

17. Fischer, I.; Kaeser, A.; Peters-Gumbs, M. A. M.; Schenning, A. P. H. J., Fluorescent π-Conjugated Polymer Dots versus Self-Assembled Small-Molecule Nanoparticles: What's the Difference? *Chemistry A European Journal* 2013, **19** (33), 10928-10934.

18. Pennakalathil, J.; Jahja, E.; Özdemir, E. S.; Konu, Ö.; Tuncel, D., Red Emitting, Cucurbituril-Capped, pH-Responsive Conjugated Oligomer-Based Nanoparticles for Drug Delivery and Cellular Imaging. *Biomacromolecules* 2014, **15** (9), 3366-3374.

19. Sun, S.; Zeng, H.; Robinson, D. B.; Raoux, S.; Rice, P. M.; Wang, S. X.; Li, G., Monodisperse MFe2O4 (M = Fe, Co, Mn) Nanoparticles. *Journal of the American Chemical Society* 2004, **126** (1), 273-279.

20. Zhang, L.; He, R.; Gu, H.-C., Oleic acid coating on the monodisperse magnetite nanoparticles. *Applied Surface Science* 2006, **253** (5), 2611-2617.

21. Massart, R., Preparation of aqueous magnetic liquids in alkaline and acidic media. *IEEE Transactions on Magnetics* 1981, **17** (2), 1247-1248.

22. Sun, S.; Zeng, H., Size-Controlled Synthesis of Magnetite Nanoparticles. *Journal of the American Chemical Society* 2002, **124** (28), 8204-8205.

23. Kallumadil, M.; Tada, M.; Nakagawa, T.; Abe, M.; Southern, P.; Pankhurst, Q. A., Suitability of commercial colloids for magnetic hyperthermia. *Journal of Magnetism and Magnetic Materials* 2009, **321** (10), 1509-1513.

24. Wildeboer, R. R.; Southern, P.; Pankhurst, Q. A., On the reliable measurement of specific absorption rates and intrinsic loss parameters in magnetic hyperthermia materials. *Journal of Physics D: Applied Physics* 2014, **47** (49), 495003.

25. Mérida, F.; Chiu-Lam, A.; Bohórquez, A. C.; Maldonado-Camargo, L.; Pérez, M.-E.; Pericchi, L.; Torres-Lugo, M.; Rinaldi, C., Optimization of synthesis and peptization steps to obtain iron oxide nanoparticles with high energy dissipation rates. *Journal of Magnetism and Magnetic Materials* 2015, **394**, 361-371.

26. Lee, J.-H.; Jang, J.-t.; Choi, J.-s.; Moon, S. H.; Noh, S.-h.; Kim, J.-w.; Kim, J.-G.; Kim, I.-S.; Park, K. I.; Cheon, J., Exchange-coupled magnetic nanoparticles for efficient heat induction. *Nature Nanotechnology* 2011, **6**, 418.

27. Lee, N.; Yoo, D.; Ling, D.; Cho, M. H.; Hyeon, T.; Cheon, J., Iron Oxide Based Nanoparticles for Multimodal Imaging and Magnetoresponsive Therapy. *Chemical Reviews* 2015, **115** (19), 10637-10689.

28. Wu, W.; Jiang, C. Z.; Roy, V. A. L., Designed synthesis and surface engineering strategies of magnetic iron oxide nanoparticles for biomedical applications. *Nanoscale* 2016, **8** (47), 19421-19474.

29. Zhang, L.; Dong, W.-F.; Sun, H.-B., Multifunctional superparamagnetic iron oxide nanoparticles: design, synthesis and biomedical photonic applications. *Nanoscale* 2013, **5** (17), 7664-7684.

30. Sivakumar, B.; Aswathy, R. G.; Romero-Aburto, R.; Mitcham, T.; Mitchel, K. A.; Nagaoka, Y.; Bouchard, R. R.; Ajayan, P. M.; Maekawa, T.; Sakthikumar, D. N., Highly versatile SPION encapsulated PLGA nanoparticles as photothermal ablators of cancer cells and as multimodal imaging agents. *Biomaterials Science* 2017, **5** (3), 432-443.

31. Béalle, G.; Di Corato, R.; Kolosnjaj-Tabi, J.; Dupuis, V.; Clément, O.; Gazeau, F.; Wilhelm, C.; Ménager, C., Ultra Magnetic Liposomes for MR Imaging, Targeting, and Hyperthermia. *Langmuir* 2012, **28** (32), 11834-11842.

View Article Online
DOI: 10.1039/D0BM00314J

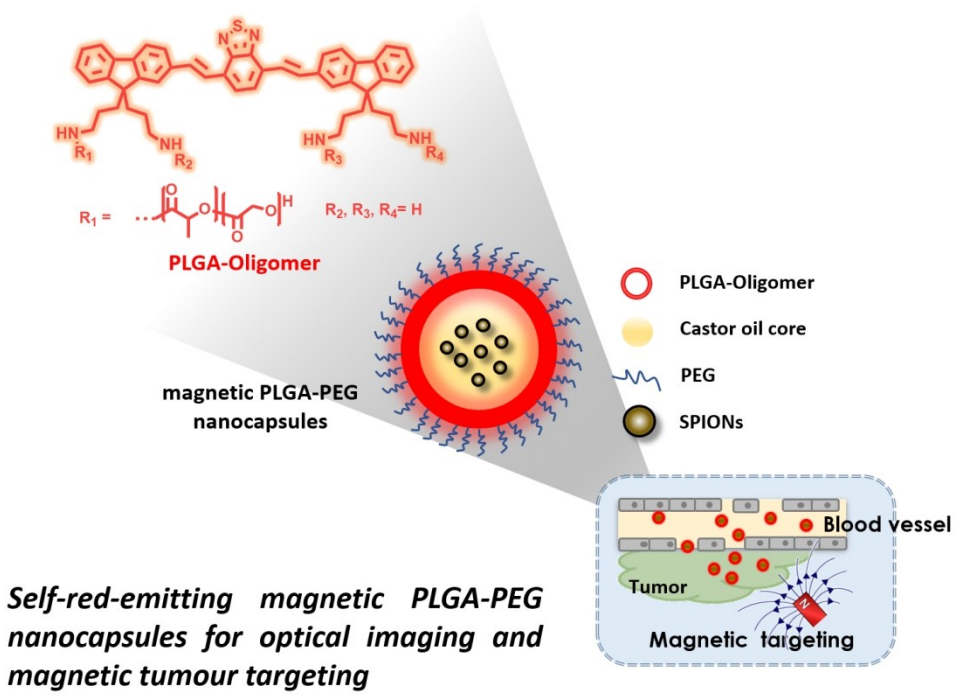

Self-red-emitting magnetic PLGA-PEG nanocapsules for optical imaging and magnetic tumour targeting

263x198mm (150 x 150 DPI)